International Journal of Thermofluids 21 (2024) 100527

Contents lists available at ScienceDirect

International Journal of Thermofluids

journal homepage: www.elsevier.com/locate/ijtf

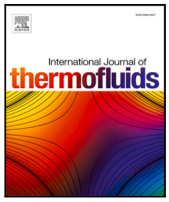

Modelling the conjugate heat transfer during the fast-filling of high-pressure hydrogen vessels for vehicular transport

C. Hall *, V. Ramasamy

University of South Wales, Pontypridd, CF37 1DL, UK

ARTICLE INFO

Keywords:
Hydrogen cylinder
Fast-filling
Heat transfer
CFD
Thermodynamic model

ABSTRACT

Compressed gas in cylinders is currently the preferred solution for storing hydrogen on board vehicles. Fast-filling combined with high storage pressures is required to meet competitive targets of long driving ranges and short refuelling times. Experiments and CFD models have shown that the fast-filling leads to significant rise in temperature within the hydrogen cylinder, which can lead to its structural failure. Thus, controlling the rise in temperature is vital during the refuelling process. This paper describes the implementation of a universal thermodynamic model that determines the gas and structural temperature during the fast-filling of hydrogen cylinders. It includes the computation of conjugate heat transfer from the gas to the cylinder structure. The thermodynamic model requires negligible computational time without compromising accuracy and can used to implement different fast-filling scenarios on a laptop or personal computer. The flexibility and robustness of the model is shown as it is capable of modelling the fast-filling of cylinders while varying different key parameters such as fill time, structural material, cylinder volume, final pressure, filling rate, initial temperatures and pressures.

1. Introduction

Hydrocarbon-based fuel vehicles are a major contributor to air pollution due to harmful emissions produced during the combustion process [1]. Increasing restrictions on transport emission regulations are driving up the demand for cleaner and more environmentally friendly fuel types. Hydrogen fuel cell vehicles utilize the energy from the gas to provide a continuous recharging process for the vehicle's battery through an electrochemical reaction [2]. This process produces zero harmful emissions, with the only by-product being water. In order to achieve a similar driving range to petrol and diesel vehicles, hydrogen gas must be stored on-board of vehicles in cylinders at relatively high pressures (35–70 MPa) [3]. The structure of cylinders on-board of hydrogen-powered vehicles consists of an inner liner to prevent leakages and an outer carbon fibre-reinforced polymer (CFRP) laminate that provides the structural strength of the cylinder [4]. Two different types of cylinders are currently used in hydrogen vehicles: Type III, which has a liner made from aluminium alloy and Type IV, whose liner is made of plastic. One of the main characteristics that needs to be adopted by hydrogen-based vehicles is a short refuelling time. Conventional vehicles can be filled in approximately three minutes and thus, hydrogen-based vehicles must provide a similar experience to meet consumer requirements. However, the fast-filling of hydrogen cylinders results in a significant rise in temperature, which can lead to structural deterioration. The rise in gas temperature is due to the negative Joule–Thompson effect that occurs upstream across the reduction valve at the pressures and temperatures involved during refuelling as well as the compression of the gas within the cylinder. [3,5–7]. Thus, for safety purposes, the maximum allowed temperature inside the vessel is set at 358 K by the International Standard Organization, while the maximum allowable pressure is 1.25 times the cylinder's design pressure [8].

The technological solution to tackle the issue of high temperature during the hydrogen refuelling process is to decrease the temperature of the gas going inside the cylinder using a heat exchanger [9,10]. The process is called pre-cooling and may be necessary to obey the hydrogen refuelling standards outlined in the SAEJ2601 protocol by the Society of Automotive Engineers. The protocol requires the cooling of the gas depending on ambient temperatures to 273 K, 253 K and 233 K throughout the fill of 70 MPa cylinders prior to being delivered on board of vehicles. [11]. In addition, the SAEJ2601 protocol explicitly states that the state of charge (SoC), which is defined as the ratio (in percentage) between the density at the end of the filling process and the density of hydrogen gas at 70 MPa and 288 K (40.2 kg/m^3) should not be greater than 100%. The SoC indicates the filling degree and it is strictly related to the temperature and pressure of the gas in the

* Corresponding author.
E-mail address: christian.hall@southwales.ac.uk (C. Hall).
URL: https://staffdirectory.southwales.ac.uk/users/christian.hall (C. Hall).

https://doi.org/10.1016/j.ijft.2023.100527
Received 14 June 2023; Received in revised form 22 November 2023; Accepted 22 November 2023
Available online 30 November 2023

Nomenclature

A_c	surface area of cylinder (m^2)
α	thermal diffusivity (m^2/s)
D_c	cylinder diameter (m)
d_{in}	inlet diameter (m)
ε	turbulence dissipation rate(m^2/s^3)
F_r	filling rate (MPa/min)
H	specific total enthalpy (J/kg)
h_{cf}	heat transfer coefficient ($W/m^2.K$)
i, j	spacial index during navigation
k_g	gas thermal conductivity (W/m K)
k_t	turbulent kinetic energy (m^2/s^2)
l	tank length (m)
m	time index during navigation
m_g	mass of gas (kg)
m_{in}	mass flow rate at the inlet (kg/s)
μ	dynamic viscosity (Pa s)
μ_t	turbulent viscosity (Pa s)
Nu	Nusselt number
p	pressure (Pa)
$\dot{q}$	heat flux (W/m^2)
$\dot{Q}_{out}$	heat transfer rate (W)
Re	Reynolds number
r	internal tank radius (m)
ρ	density (kg/m^3)
T	temperature (K)
t	time (s)
u	velocity (m/s)
u_g	specific internal energy (J/kg)
V_c	cylinder volume (L)
x	spatial horizontal distance (m)
y	spatial vertical distance (m)

cylinder. A high value very close to 100% is desirable since it provides a larger driving range. However, pre-cooling of the gas requires energy. Thus, it imperative to determine the least amount of energy input that is required to lower the gas temperature for cost savings.

The experimental investigation of the fast-filling process of hydrogen gas within cylinders requires vast amounts of resources and time. Thus, computational fluid dynamics (CFD) models have been developed to simulate fast-filling of hydrogen cylinders [3–6,9,10,12–21]. Those computational models include both two-dimensional axisymmetric and fully three-dimensional unsteady Reynolds-averaged Navier–Stokes simulations. Experiments have shown that fast-filling of hydrogen cylinders provides a relatively uniform gas temperature. A maximum temperature variation of 5 K is seen across multiple experiments when the refilling time is below 3 min [10,22]. Extension of the refilling duration beyond 3 min increases the thermal stratification of the gas resulting in larger temperature variations [22]. It has also been shown that larger cylinders lead to increased stratification of the gas [16]. Thus, fully three-dimensional simulations may be more suited to extended refilling durations and large cylinders above 74 L. A study by Suryan et al. [19] showed that the two-equation standard k-ε turbulence model [23] is best suited to simulate the fast-filling of hydrogen cylinders when considering accuracy, computational time and convergence when compared to different turbulence models. Furthermore, CFD simulations [3,6,10,12,21] have shown that axisymmetric simulations along with the two-equation standard k-ε turbulence model [23] accurately predicts the rise in gas temperature throughout the fill. However, multidimensional CFD simulations of the filling process is computationally expensive due to the unsteadiness of the flow, the requirement of a real gas equation of state and the calculation of the conjugate heat transfer from the gas to the structure of the cylinder. Thus, the computational cost associated with CFD models along with the requirement of an experienced CFD user motivates the need for a low-order thermodynamic model that can determine the gas temperature in the cylinder during the filling without compromising accuracy. Monde et al. [24] developed a thermodynamic model whereby it was determined that the heat transfer coefficient should have a constant value of 500 $W/(m^2K)$ throughout the fill to match their experimental results that involved the fast-filling of a 1.38 L cylinder to 35 MPa. The size of the cylinder used by Monde et al. [24] is not representative of actual cylinder sizes in hydrogen-powered vehicles such as the Toyota Mirai [25] that requires of two cylinders for a total volume of 122.4 L. Similarly, the model developed by Striednig et al. [26] on a 23.5 L Type I cylinder (all-metal with no laminate) is atypical of real case scenarios. In their model, Striednig et al. [26] assumed that the heat transfer coefficient from the gas to the cylinder wall is similar to turbulent pipe flows and modelled the Nusselt number using a modified version of the correlation developed by Petukhov [27]. Thermodynamic models developed by Johnson et al. [15] and Woodfield et al. [28] included both forced and free convection for heat transfer from the gas to the structure of the cylinder. However, experiments and the resulting model performed by Bourgeois et al. [21] showed that free convection plays a negligible role in heat transfer during the filling process, which is similar to the assumptions made by Ramasamy et al. [3].

A review of the thermodynamic models [3,15,21,24,26,28] show that each model has only been tested for a specific cylinder size, structure, final pressure and fill time. The objective of this present study is to develop a thermodynamic model that is valid for cylinders of different sizes, materials, final pressures and fill times. Initially, a two-dimensional axisymmetric analysis of the filling process of a 74 L Type III cylinder from an initial pressure of 9.36 MPa to a final value of 35 MPa is performed, which will be validated using experimental data [12]. The CFD analysis will be used to model the Nusselt number based on the inlet Reynolds number. Following the CFD simulation, a zero-dimensional thermodynamic filling model coupled with a one-dimensional heat transfer across the structure will be used to validate the Nusselt number relationship for different filling conditions.

2. Methodology

2.1. CFD simulation

Governing equations

The CFD model assumes that buoyancy is negligible when compared to the inertial effects during the filling process. Thus, a two-dimensional axisymmetric CFD model is used to simulate the fill using the FLUENT software package. The unsteady compressible Reynolds-Averaged Navier–Stokes (RANS) equations (Eqs. (1)–(3)) are used to determine the flow field and gas temperature throughout the fill.

$$\frac{\partial \bar{\rho}}{\partial t} + \frac{\partial (\bar{\rho}\tilde{u})}{\partial x_i} = 0 \tag{1}$$

$$\frac{\partial (\bar{\rho}\tilde{u}_i)}{\partial t} + \frac{\partial (\bar{\rho}\tilde{u}_i\tilde{u}_j)}{\partial x_j} = -\frac{\partial \bar{p}}{\partial x_i} + \frac{\partial}{\partial x_j}\left(\bar{\tau}_{ij} - \overline{\rho u'_i u'_j}\right) \tag{2}$$

$$\frac{\partial (\bar{\rho}\tilde{H}_i)}{\partial t} + \frac{\partial (\bar{\rho}\tilde{H}\tilde{u}_j)}{\partial x_j} = -\frac{\partial \bar{p}}{\partial t} + \frac{\partial}{\partial x_j}\left(\bar{q}_j - \overline{\rho h' u'_j} + \tilde{u}_i\bar{\tau}_{ij} + \overline{u'_i\tau_{ij}}\right) \tag{3}$$

where $\tilde{u}$ is the Favre-averaged velocity, $\bar{\rho}$ is the ensemble-averaged density and $\bar{\tau}_{ij}$ is the stress tensor. Unclosed terms that appear in either the momentum equation (Eq. (2)) or energy equation (Eq. (3)): $\overline{\rho u'_i u'_j}$, $\overline{\rho h' u'_j}$ and $\overline{u'_i\tau_{ij}}$ are modelled using the k-ε turbulence model [23]. The k-ε model uses the partial differential equations of the transport of the turbulent kinetic energy per unit mass (k_t) and the dissipation rate per

unit mass (ε). The two-transport equations implemented in FLUENT are as follows:

$$\frac{\partial(\rho k_t)}{\partial t} + \frac{\partial(\rho k_t u_i)}{\partial x_i} = \frac{\partial}{\partial x_j}\left[\left(\mu + \frac{\mu_t}{\sigma_k}\right)\frac{\partial k_t}{\partial x_j}\right] + \mu_t S^2 - \rho\varepsilon - 2\rho\varepsilon\frac{k_t}{{c_s}^2} \quad (4)$$

$$\frac{\partial(\rho\varepsilon)}{\partial t} + \frac{\partial(\rho\varepsilon u_i)}{\partial x_i} = \frac{\partial}{\partial x_j}\left[\left(\mu + \frac{\mu_t}{\sigma_\varepsilon}\right)\frac{\partial\varepsilon}{\partial x_j}\right] + C_{1\varepsilon}\frac{\varepsilon}{k_t}\mu_t S^2 - C_{2\varepsilon}\rho\frac{\varepsilon^2}{k_t} \quad (5)$$

where μ is the dynamic viscosity, the terms σ_k and σ_ε are the turbulent Prandtl numbers for k_t and ε respectively. The values of σ_k and σ_ε were respectively set to 1 and 0.85. $C_{1\varepsilon}$ and $C_{2\varepsilon}$ are constants with given values of 1.44 and 1.92 respectively. c_s is the speed of sound, S is the modulus of the mean rate-of-strain tensor and μ_t is the eddy viscosity (Eq. (6)).

$$\mu_t = \bar{\rho} C_\mu \frac{k_t^2}{\varepsilon} \quad (6)$$

where C_μ is a default constant of the k-ε turbulence model and has a value of 0.09.

Equation of State

An equation of state is required to close the governing and turbulence model equations (Eqs. (1)–(5)). Real gas effects are significant at the pressures and temperatures involved during the fast-filling of hydrogen cylinders and the gas is expected to deviate from ideal gas behaviour. The real gas equation chosen for the simulation in this study is the Helmholtz equation of state for hydrogen [29], which is obtained from the NIST database: REFPROP 10.0.

Molecular viscosity & Thermal conductivity

Gas properties such as molecular viscosity and thermal conductivity are not constant throughout the filling process due to the effects of compressibility. The values of those properties are updated throughout the fill and are also obtained from REFPROP 10.0. The empirical correlations of Muzny et al. [30] and Assael et al. [31] are used to respectively determine the viscosity and thermal conductivity of the gas throughout the filling process.

Cylinder geometry & Computational grid

The dimensions and material properties of the cylinder are obtained from Dicken and Mérida [12] (Tables 1 & 2). Isotropic material properties are assumed for the structure of the cylinder. In addition, it is assumed that both the liner and the laminate have a uniform thickness and that their respective thermal properties are unaffected by changes in temperature. The two-dimensional axisymmetric geometry of the cylinder is divided into a fluid domain that consists of the hydrogen gas and a solid domain that includes both the liner and the laminate (Fig. 1). The simulations employ a hybrid mesh consisting of both structured and unstructured grids. Structured grids are used to discretize the liner and laminate, to resolve the viscous sublayer at the interface between the gas and liner such that the maximum non-dimensional y^+ value is less than one. In a addition, a refined structured mesh is used to capture the incoming jet into the cylinder, while the rest of the fluid domain is discretized with an unstructured mesh.

Numerical set-up

Initial conditions of pressure and temperature of the hydrogen gas are assumed to be uniform throughout the cylinder and have values of 9.36 MPa and 293.4 K respectively, which are similar to experimental values of Dicken and Mérida [12]. It is also assumed that the structural materials of the cylinder are initially in thermal equilibrium with the gas. The no slip boundary condition (v = 0 m/s) is employed at the interface between the gas and the liner. The total temperature and pressure profiles at the inlet (Fig. 2(a)) are loaded as text files to match the experimental data of Dicken and Mérida [12]. At the outer wall of the laminate, adiabatic conditions are applied since it assumed that the fast-filling coupled with the relatively low thermal conductivity of the laminate will lead to negligible heat transfer to the atmosphere. The axis boundary condition is applied to the centreline of the cylinder due to its axisymmetric geometry.

Table 1
Dimension of the cylinder [12].

Description	Dimension (m)
Length of tank	0.893
Inner radius of tank	0.179
Outer radius of tank	0.198
Liner thickness	0.004
Laminate thickness	0.015
Inner diameter of inlet tube	0.005
Thickness of tube wall	0.002
Length of tube protruding into tank	0.082

Table 2
Material properties of the cylinder [12].

	Liner	Laminate
Density (kg/m^3)	2730	1494
Specific heat (J/kg K)	900	938
Thermal conductivity (W/m K)	167	1.0

Table 3
Coordinate location of local gas temperature measurements 20 s into the fill.

Location	x/l	y/r
T_1	0.2	0.77
T_2	0.46	0.89
T_3	0.83	0.81
T_4	0.84	0.33

The CFD simulation is carried out using the pressure-based solver with an implicit scheme. Convergence of the solution at each time step is monitored by ensuring that the average heat flux from the gas to the structure of the cylinder no longer changes for each time step. A time step of 10^{-4} s is chosen after confirming that reducing the time step to 10^{-5} s no longer changes the solution.

Grid independence is determined by considering the mass-averaged gas temperature during the fill. The grid distances within the fluid domain are adjusted such that the total cell counts are 20,000, 36,000, 50,000 and 100,000. Following the mesh sensitivity analysis, 36,000 cells are used for the discretization of the axisymmetric domain of the cylinder, since further increasing the cell count no longer significantly changes the mass-averaged gas temperature throughout the fill (Fig. 2(b)). Data for the local gas temperatures is only available at 20 s into the fill as opposed to its entire duration. The CFD model is further validated by comparing the local gas temperatures that were obtained from the CFD model to the experimental data 20 s into the fill at four different locations within the cylinder [22]. Those particular locations are shown in Fig. 1 (T_1, T_2, T_3 & T_4) and the coordinates provided in Table 3.

2.2. Thermodynamic model

The thermodynamic model is coded in the MATLAB software. The governing equations used in the model are the mass conservation and energy equations (Eqs. (7) & (8)).

$$\frac{dm_g}{dt} = \dot{m}_{in} \quad (7)$$

where m_g is the evolution of the mass of the gas in the cylinder during the fill, $\dot{m}_{in}$ is the mass flow rate of the gas at the inlet.

$$\frac{d(m_g u_g)}{dt} = \dot{m}_{in} H_{in} + \dot{Q}_{out} \quad (8)$$

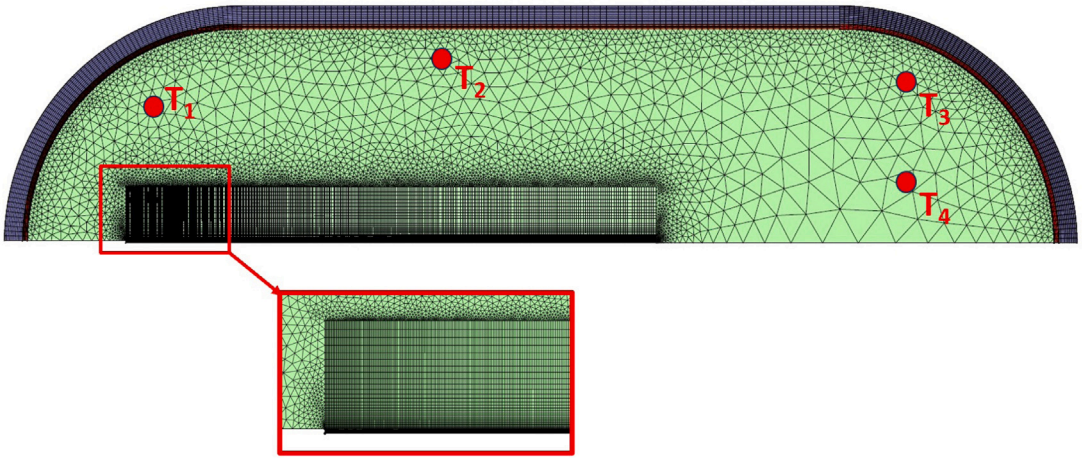

Fig. 1. Axisymmetric computational grid of the cylinder.

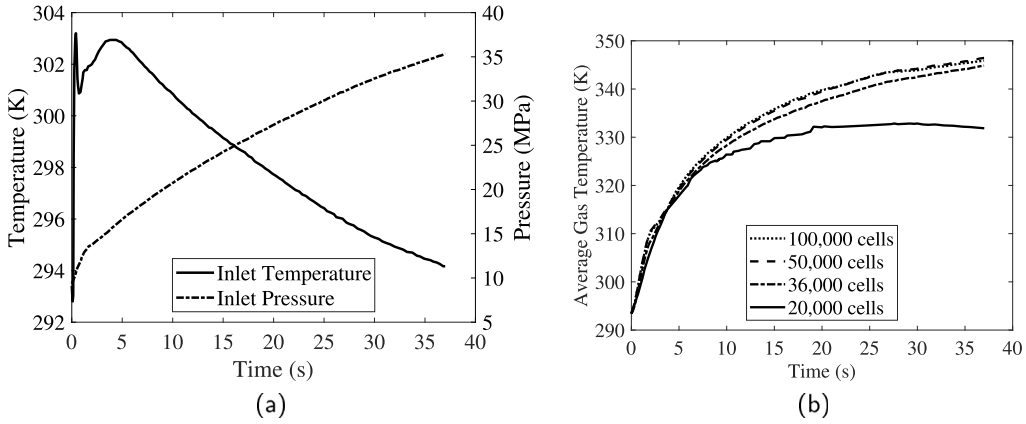

Fig. 2. (a) Inlet pressure and temperature boundary conditions [12], (b) Mesh independence test.

where u_g is the specific internal energy of the gas within the cylinder, H_{in} is the total enthalpy at the inlet and $\dot{Q}_{out}$ is the heat transfer rate from the gas to the structure of the cylinder.

The model requires the value of the gas temperature at the inlet before it enters the cylinder. In addition, for cases whereby the mass flow rate is unknown, its value is determined using the difference between the upstream inlet pressure and gas pressure. Similar to the CFD case, the thermodynamic model uses the Helmholtz equation of state for hydrogen [29] from REFPROP 10.0 to determine gas properties such as the specific internal energy, temperature, viscosity thermal conductivity and pressure throughout the fill. The velocity of the gas entering the cylinder at any point during the fill is determined from the mass flow rate (Eq. (9)).

$$u_{in} = \frac{\dot{m}}{\rho \times A_{in}} \tag{9}$$

where ρ is the density of the gas entering the cylinder and is determined using REPFROP 10.0 since it is a function of the inlet gas temperature and pressure (Eq. (10)). A_{in} is the cross-sectional area of the inlet.

$$\rho = \rho(P_0, T_0) \tag{10}$$

where P_0 and T_0 are the inlet pressure and temperature at any time during the fill.

The heat transfer rate in Eq. (8) is calculated by multiplying the heat flux ($\dot{q}$) by the internal surface area (A_c) of the cylinder (Eq. (11)).

$$\dot{Q}_{out} = \dot{q} \times A_c \tag{11}$$

The heat flux ($\dot{q}$) is determined using Eq. (12).

$$\dot{q} = h_{cf}(T_w - T_g) \tag{12}$$

where h_{cf} is the heat transfer coefficient that is calculated in Eq. (13). T_w and T_g are respectively the internal wall and gas temperatures. Nu is the Nusselt number and its value is updated throughout the fill using a Reynolds number/Nusselt number relationship that is derived from the CFD model. The variables D_c and k_g in Eq. (13) are the internal diameter of the cylinder and the thermal conductivity of the gas respectively.

$$Nu = \frac{h_{cf} D_c}{k_g} \tag{13}$$

A one-dimensional heat transfer model is applied normal to the structure of the cylinder (Fig. 3). The structural material of the cylinder consists of layers of the liner and laminate, with uniform thickness and constant material properties throughout the fill. The one-dimensional heat equation (Eq. (14)) is used to determine the temperature of across the structure.

$$\frac{\partial T}{\partial t} = \alpha \frac{\partial^2 T}{\partial x^2} \tag{14}$$

where T is the structural temperature and α is the thermal diffusivity, which is given in Eq. (15).

$$\alpha = \frac{k}{\rho c} \tag{15}$$

where k is the thermal conductivity, ρ is the density and c is the specific heat of either the liner or laminate. The material properties of the cylinders that are used in both the CFD simulation and the thermodynamic model are shown in Table 4.

The one-dimensional heat equation (Eq. (14)) is solved using the explicit forward Euler scheme (Eq. (16)) to determine the temperature

Table 4
Material properties of the liner and laminate [5].

Cylinder	Cylinder structure	Material	Specific heat, J/kg K	Thermal conductivity, W/m K	Density, kg/m^3
Type III	Liner	Aluminium	900	167	2730
	Laminate	CFRP	938	1	1494
Type IV	Liner	Plastic	1880	0.36	947
	Laminate	CFRP	1400	1.5	1600

Table 5
Hydrogen fast-filling case studies.

Case	Cylinder volume, L	Cylinder type	Initial pressure, MPa	Final pressure, MPa	Initial temperature, K	Inlet diameter, mm
1. Johnson et al. [15]	36.9	IV	0.14	13.79	296.5	5
2. Melideo et al. [16]	28.9	IV	2	77.5	288	3
3. Zheng et al. [10]	74.3	III	5.5	63.3	289	5

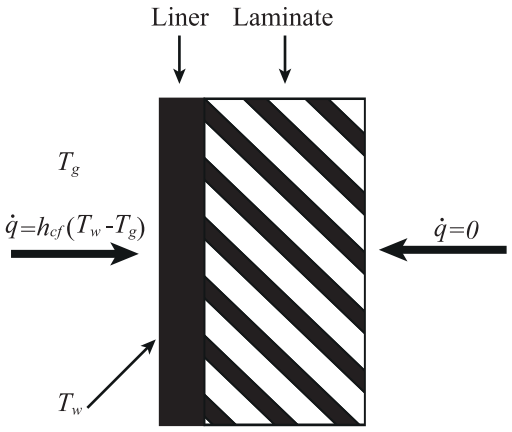

Fig. 3. One-dimensional heat transfer schematic representation.

across the structure of the cylinder.

$$T_i^{m+1} = T_i^m + \frac{\alpha \Delta t}{(\Delta x)^2}\left(T_{i-1}^m - 2T_i^m + T_{i+1}^m\right) \tag{16}$$

where Δt and Δx are the respective temporal and spatial discretization. Eq. (16) is only valid if the stability criteria ($0 \leq \frac{\alpha \Delta t}{(\Delta x)^2} \leq 0.5$) is satisfied.

2.3. Case studies

The thermodynamic model is calibrated using the relationship that is obtained from the CFD model between the inlet Reynolds number (Eq. (17)) and Nusselt number (Eq. (13)) to determine heat transfer from the gas to the structure of the cylinder. The same Reynolds Number/Nusselt number relationship will used for three different filling scenarios, which are outlined in Table 5 to validate the thermodynamic model. The inlet pressure and temperature boundary conditions for all three cases are displayed in Fig. 4.

$$Re = \frac{\rho u_{in} d_{in}}{\mu} \tag{17}$$

where u_{in} is the velocity of the gas at the inlet and d_{in} is the inlet diameter.

3. Results

3.1. CFD

Results from the CFD simulation show that the two-equation standard k-ε turbulence model is capable of predicting the mass-averaged gas temperature profile during the fill (Fig. 5). The CFD model accurately predicts the sharp rise in the gas temperature at the start of the fill, which is mainly due to the negative Joule–Thompson effect. The model slightly over-predicts the mass-averaged gas temperature from five seconds onwards into the fill and the final gas temperature is 344.5 K according to the simulations as opposed to 342 K from the experiment. This represents a percentage error of 5% in the determination of the final gas temperature based on a baseline temperature of 293.4 K that is similar to the initial conditions. A comparison of the local gas temperatures at four different locations within the cylinder (Fig. 1) at 20 s into the fill shows a strong conformity between the experimental and CFD results (Table 6). The highest deviation is 1.7 K at location T_1, which represents a percentage error of 3.5% and leads to further validation of the CFD model.

Table 6
Local gas temperatures 20 s into the fill.

Location	Expt gas temp (K) [22]	CFD gas temp (K)
T_1	339.2	337.5
T_2	336.1	337.6
T_3	337.2	337.6
T_4	337.3	337.4

Fig. 6 shows the flow-field superimposed over contours of the gas temperature at different times throughout the fill. The gas entering the cylinder impinges on the surface opposite to the inlet and recirculates. The recirculating pattern is similar at different times during the fill and results in large-scale mixing, which explains the homogeneity of the gas temperature in the cylinder. This is consistent with the findings of Ramasamy et al. [6] who found that the recirculating flow field is self-similar throughout the fill when the length to inner-diameter ratio of the cylinder is less than 3. When the length to inner-diameter ratio exceeds 3, there is a lack of flow recirculation further downstream that leads to hot spots near the end of the cylinder. A sharp rise in the mass flow rate of the gas entering the cylinder is observed during the first two seconds of the fill (Fig. 7(a)). Following the initial two-second time period, the mass flow rate decreases throughout the rest of the filling process. In addition, the CFD model shows that the profile of the area-averaged heat flux at the inner surface of the cylinder during the fill is quasi-similar to that of the mass flow rate. This finding suggests that the convective heat transfer coefficient at the inner wall is dependent upon the mass flow rate. The Nusselt number, which is representative of the convective heat transfer at the interface between the gas and the inner surface of the cylinder is plotted against inlet Reynolds number (Fig. 7(b)). A power relationship (Eq. (18)) is obtained between the Reynolds number and the Nusselt number that will enable the calculation of the heat transfer coefficient in the thermodynamic model.

$$Nu = aRe^b \qquad 0 \leq Re \leq 2.5 \times 10^6 \tag{18}$$

where $a = 3.3 \times 10^{-4}$ and $b = 1.18$.

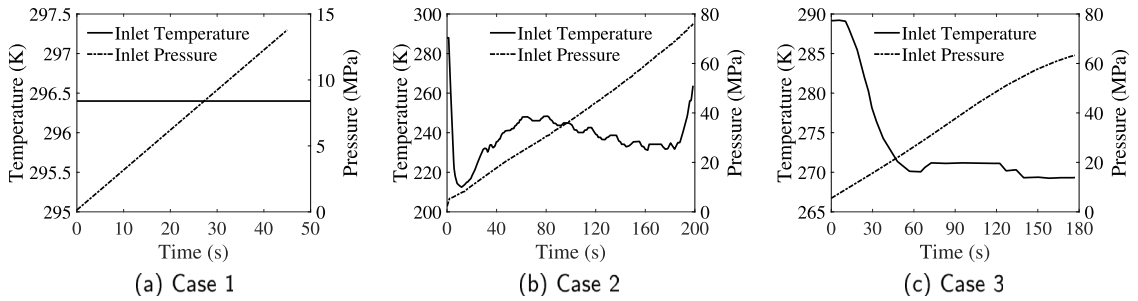

Fig. 4. Inlet pressure and temperature boundary conditions.

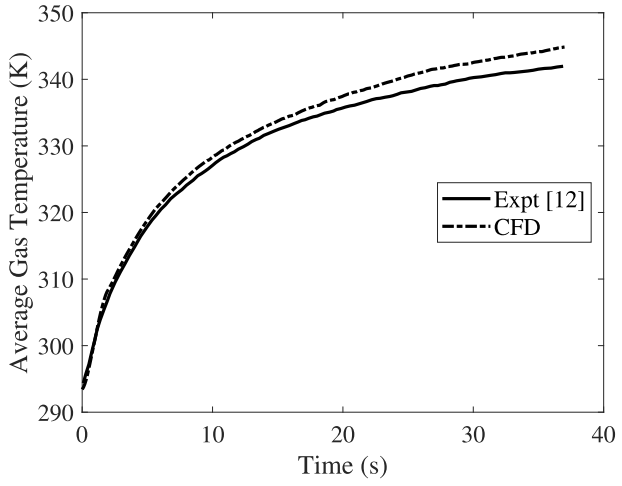

Fig. 5. Comparison of the mass-averaged gas temperature (CFD v/s Expt [12]).

3.2. Thermodynamic model

The thermodynamic model is calibrated using the power relationship between the Reynolds number and Nusselt number (Eq. (18)). Fig. 8(a) shows that the thermodynamic model (T-Model) overestimates the gas temperature throughout the fill. The highest overestimation occurs at 3 s into the fill whereby the T-model over-predicts the gas temperature by 4 K. However, the profile of the gas temperature obtained from the T-Model is similar to the profiles of both the CFD and experiment. A sharp rise in the gas temperature is obtained at the start due to the negative Joule–Thomson effect at the corresponding filling pressure and temperature of hydrogen gas. As the filling proceeds, a gradual increase in the gas temperature is observed, which is mainly due to the compression of the gas in the cylinder. The final gas temperature according to the T-Model is 345.5 K, compared to 344.5 K from the CFD and 342 K according to the experiment of Dicken and Mérida [12]. Moreover, while a difference of 1 K is observed in the final gas temperature, the computational time of the T-Model is significantly lower at 18 s when compared to the CFD, which required 272 h (Table 7). An adiabatic filling scenario using the T-Model whereby no heat is transferred from the gas to the structure, shows that the gas temperature of the gas significantly higher and has a final value of 381.5 K (Fig. 8(b)). This further confirms that the fast-filling process is non-adiabatic and its modelling requires conjugate heat transfer from the gas to the structural material of the cylinder.

Fig. 9 shows the progression of the gas temperature according to the thermodynamic model for the different fast-filling case studies that are described in Table 5. In all 3 cases, the T-model, shows a rise in the gas temperature in the cylinder throughout the fill, which is in accordance with the respective experimental data. The largest discrepancy in the gas temperature profiles is observed at the start of

Table 7
Final gas temperature and computational time comparison.

	Final avg. temperature, K	Computational time, h
1. Experiment [12]	342	–
2. CFD	344.5	272
3. Thermodynamic Model (T-Model)	345.5	0.005

the fill between the T-Model and the experimental data of Johnson et al. [15] (Fig. 9(a)). However, as the filling proceeds, the temperature curves coincide and a difference of only 1 K is observed at the end of the 45 s fill. Comparison of the final gas temperatures for each case and the respective percentage errors and computational times are shown in Table 8. The maximum percentage error in determining the final gas temperature is 3.5%, which occurs when modelling the 200 s filling case of Melideo et al. [16]. According to Melideo et al. [16], their 3D CFD model required several weeks for completion as opposed to a computational time of 222 s for the T-Model. The range of relevant parameters for which the T-Model has been tested and validated is outlined in Table 9.

The gas temperature profiles of the T-Model in Fig. 9 assume that no heat transfer occurs at the outer wall of the cylinders during the fast-fill. Further simulations of the 3 cases are performed using the T-model whereby isothermal conditions are considered on the outer walls of the cylinders. The outer wall temperatures are kept a constant value, similar to the respective initial ambient conditions throughout the fill. An isothermal wall condition is chosen, since it represents the extreme case for maximum heat transfer to the atmosphere. Fig. 10 shows that in all 3 cases, the boundary condition at the outer wall of the laminate does not influence the gas temperature during the fast-fill. The relatively low thermal conductivity of the laminate acts as a barrier for heat transfer from the structure of the cylinder to the atmosphere during the fast-fill (Fig. 11). Case 3 involves the fast-filling of a type III cylinder and a uniform temperature in the aluminium liner occurs throughout the duration of fill (Fig. 11(c)). This is due to its relatively high thermal conductivity as opposed to the laminate (167 W/m K v/s 1 W/m K). A type IV cylinder is used for the fast-filling in cases 2 and 3. A temperature gradient is observed along the thickness of the plastic liner throughout the fill due to its relatively low thermal conductivity. A similar gradient in the material temperature can be noticed across the thickness of the laminate.

4. Conclusions

The following conclusions can be drawn from this current study:

- The standard k-ϵ turbulence model accurately predicts the rise in gas temperature during the fast-filling of a Type III hydrogen cylinder and is used to develop a relationship between the Nusselt number and the inlet Reynolds number.

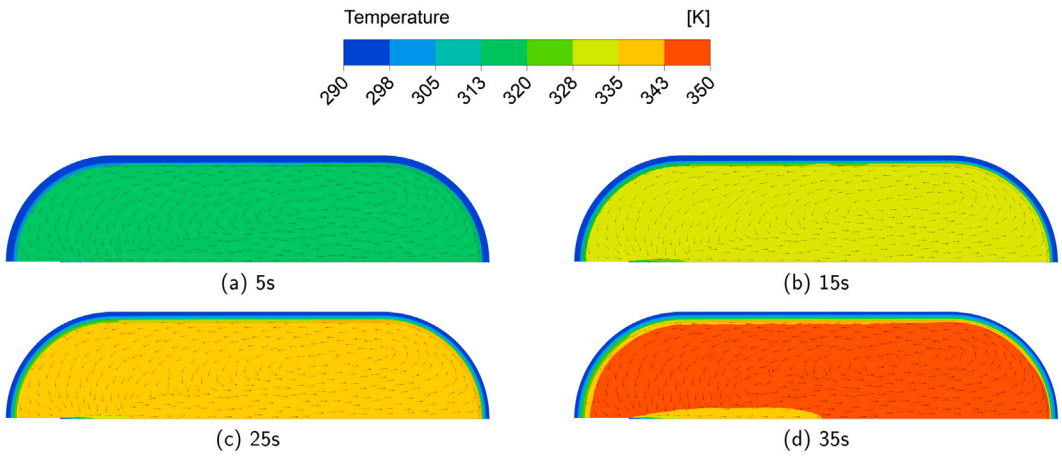

Fig. 6. Flow-field superimposed over gas and structural temperature at different times during the fill.

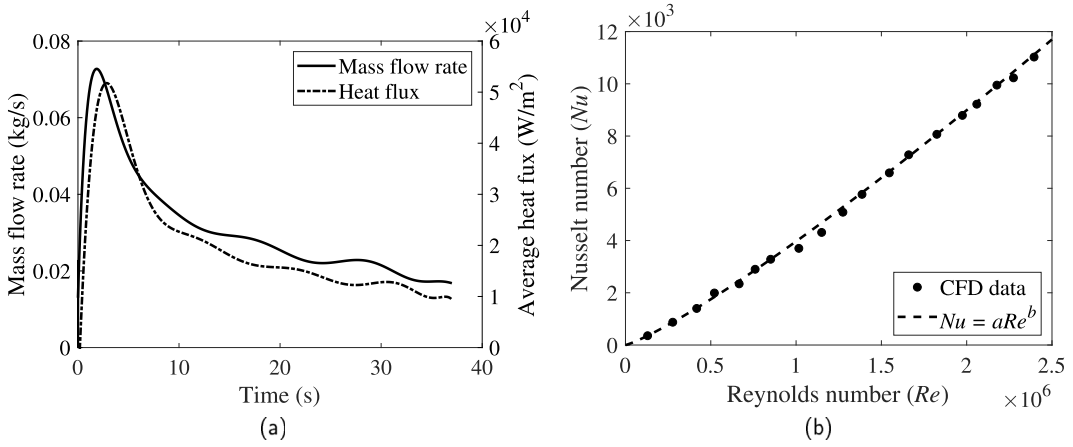

Fig. 7. (a) Mass flow rate and heat flux computation during the fill, (b) Reynolds number/Nusselt number relationship.

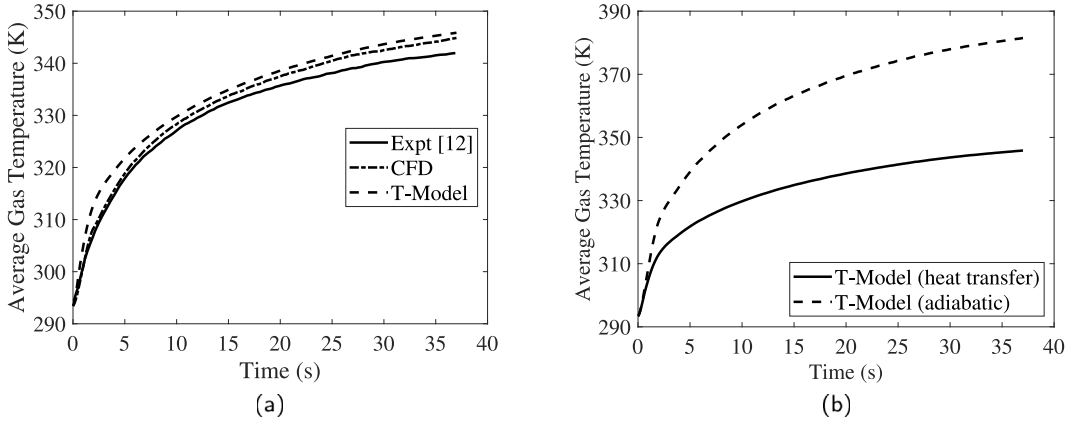

Fig. 8. (a) Comparison of the mass-averaged gas temperature profiles, (b) Comparison of the mass-averaged gas temperature in the cylinder with conjugate heat transfer and adiabatic wall conditions.

Table 8
T-Model results.

Case	Final avg. temperature (Expt), K	Final avg. temperature (T-Model), K	Percentage error, %	Computational time, s
1. Johnson et al. [15]	360	361	1.5	45
2. Melideo et al. [16]	330.5	332	3.5	222
3. Zheng et al. [10]	332	332	0	202

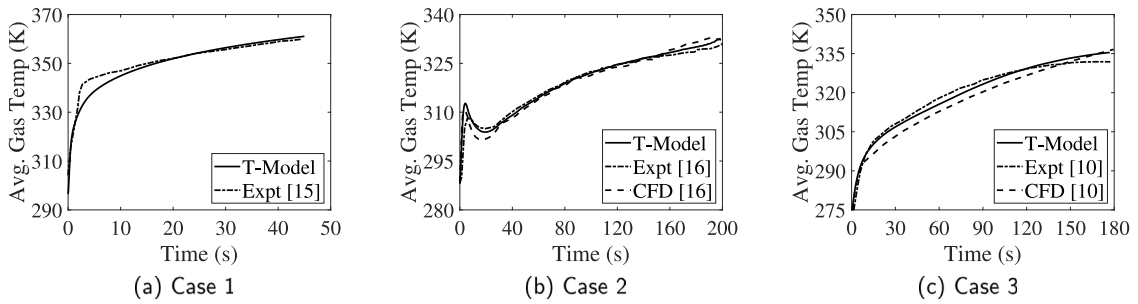

Fig. 9. Comparison of the mass-averaged gas temperature profiles: (a) T-Model v/s Johnson et al. [15], (b) T-Model v/s Melideo et al. [16], T-Model v/s Zheng et al. [10].

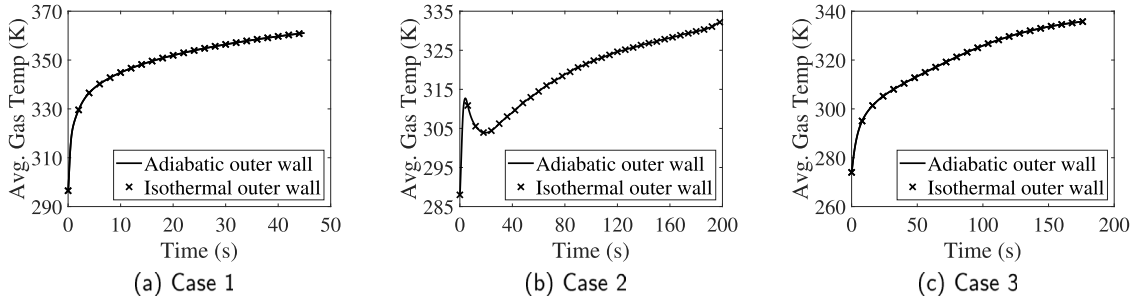

Fig. 10. Comparison of the gas temperature profiles with adiabatic and isothermal outer wall boundary conditions.

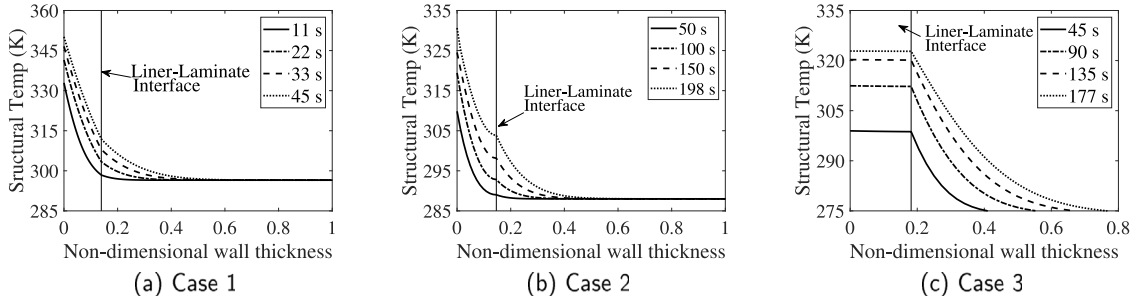

Fig. 11. Comparison of the profiles of the structural temperature using the T-Model for the different case studies during the respective fills.

Table 9
Tested and validated parameters of T-Model.

Parameters	
Cylinder type	III, IV
Cylinder volume (V_c), L	$28.9 \leq V_c \leq 74$
Final pressure (P), MPa	$13.79 \leq P \leq 77.5$
Filling time (t), s	$37 \leq t \leq 200$
Filling rate (F_r), MPa/min	$18.2 \leq F_r \leq 41.6$
Inlet Reynolds number (Re)	$0 \leq Re \leq 2.5 \times 10^6$

- The CFD model shows the development of a self-similar recirculating flow field within the cylinder, that mixes the gas during refuelling, resulting in a uniform gas temperature throughout the cylinder.
- The Reynolds number/Nusselt number relationship is implemented in a thermodynamic model, which has shown its ability to predict the gas temperature profiles in both Type III and IV cylinders that have different volumes. In addition to those parameters, the T-Model has shown its flexibility in predicting the gas temperature for different fill times, fill rates and final pressures.
- The 0D T-Model significantly reduces the computational time to the order of tens/hundreds of seconds as opposed to days/weeks for conventional CFD models. The T-Model is tool that can be used to determine the average gas temperature in the cylinder during the fast-filling. However, the T-model cannot determine local gas temperatures as opposed to CFD.
- Heat transfer from the structure of the cylinder to the atmosphere is negligible during the fast-fill, due to the relatively low thermal conductivity of the laminate.

CRediT authorship contribution statement

C. Hall: Conceptualization, Writing – original draft. **V. Ramasamy:** Supervision, Writing – review & editing.

Declaration of competing interest

The authors declare that they have no known competing financial interests or personal relationships that could have appeared to influence the work reported in this paper.

Data availability

Data will be made available on request.

References

[1] S. Akansu, Z. Dulger, N. Kahraman, T. Veziroğlu, Internal combustion engines fueled by natural gas—hydrogen mixtures, Int. J. Hydrogen Energy 29 (14) (2004) 1527–1539.

[2] S. Peighambardoust, S. Rowshanzamir, M. Amjadi, Review of the proton exchange membranes for fuel cell applications, Int. J. Hydrogen Energy 35 (17) (2010) 9349–9384.

[3] V. Ramasamy, E. Richardson, P. Reed, W. Hepples, A. Wheeler, Investigating the use of phase-change materials for temperature control during fast filling of hydrogen cylinders, High Temp. Mater. Process. Int. Q. High-Technol. Plasma Process. 22 (2–3) (2018) 73–97.

[4] S. Kim, S.H. Lee, K. Yoon, Thermal characteristics during hydrogen fueling process of type iv cylinder, Int. J. Hydrogen Energy 35 (13) (2010) 6830–6835.

[5] A. Suryan, H.D. Kim, T. Setoguchi, Three dimensional numerical computations on the fast filling of a hydrogen tank under different conditions, Int. J. Hydrogen Energy 37 (9) (2012) 7600–7611.

[6] V. Ramasamy, E. Richardson, Thermal response of high-aspect-ratio hydrogen cylinders undergoing fast-filling, Int. J. Heat Mass Transfer 160 (2020) 120179.

[7] J.-Q. Li, Y. Chen, Y.B. Ma, J.-T. Kwon, H. Xu, J.-C. Li, A study on the joule-thomson effect of during filling hydrogen in high pressure tank, Case Stud. Therm. Eng. 41 (2023) 102678.

[8] Gaseous Hydrogen and Hydrogen Blends- Land Vehicle Fuel Tanks, Standard, International Organization for Standardization, Geneva, CH, 2009.

[9] D. Melideo, D. Baraldi, N.D.M. Echevarria, B.A. Iborra, Effects of some key-parameters on the thermal stratification in hydrogen tanks during the filling process, Int. J. Hydrogen Energy 44 (26) (2019) 13569–13582.

[10] J. Zheng, J. Guo, J. Yang, Y. Zhao, L. Zhao, X. Pan, J. Ma, L. Zhang, Experimental and numerical study on temperature rise within a 70 MPa type III cylinder during fast refueling, Int. J. Hydrogen Energy 38 (25) (2013) 10956–10962.

[11] SAE International, Fueling Protocols for Light Duty Gaseous Hydrogen Surface Vehicles, Tech. Rep., 2020.

[12] C.J.B. Dicken, W. Mérida, Modeling the transient temperature distribution within a hydrogen cylinder during refueling, Numer. Heat Transfer A 53 (7) (2007) 685–708.

[13] M.C. Galassi, D. Baraldi, B.A. Iborra, P. Moretto, CFD analysis of fast filling scenarios for 70 MPa hydrogen type IV tanks, Int. J. Hydrogen Energy 37 (8) (2012) 6886–6892.

[14] M.C. Galassi, E. Papanikolaou, M. Heitsch, D. Baraldi, B.A. Iborra, P. Moretto, Assessment of CFD models for hydrogen fast filling simulations, Int. J. Hydrogen Energy 39 (11) (2014) 6252–6260.

[15] T. Johnson, R. Bozinoski, J. Ye, G. Sartor, J. Zheng, J. Yang, Thermal model development and validation for rapid filling of high pressure hydrogen tanks, Int. J. Hydrogen Energy 40 (31) (2015) 9803–9814.

[16] D. Melideo, D. Baraldi, M.C. Galassi, R.O. Cebolla, B.A. Iborra, P. Moretto, CFD model performance benchmark of fast filling simulations of hydrogen tanks with pre-cooling, Int. J. Hydrogen Energy 39 (9) (2014) 4389–4395.

[17] D. Melideo, D. Baraldi, CFD analysis of fast filling strategies for hydrogen tanks and their effects on key-parameters, Int. J. Hydrogen Energy 40 (1) (2015) 735–745.

[18] L. Wang, C. Zheng, S. Wei, B. Wang, Z. Wei, Thermo-mechanical investigation of composite high-pressure hydrogen storage cylinder during fast filling, Int. J. Hydrogen Energy 40 (21) (2015) 6853–6859.

[19] A. Suryan, H.D. Kim, T. Setoguchi, Comparative study of turbulence models performance for refueling of compressed hydrogen tanks, Int. J. Hydrogen Energy 38 (22) (2013) 9562–9569.

[20] J. Liu, S. Zheng, Z. Zhang, J. Zheng, Y. Zhao, Numerical study on the fast filling of on-bus gaseous hydrogen storage cylinder, Int. J. Hydrogen Energy 45 (15) (2020) 9241–9251.

[21] T. Bourgeois, T. Brachmann, F. Barth, F. Ammouri, D. Baraldi, D. Melideo, B. Acosta-Iborra, D. Zaepffel, D. Saury, D. Lemonnier, Optimization of hydrogen vehicle refuelling requirements, Int. J. Hydrogen Energy 42 (19) (2017) 13789–13809.

[22] C.J.B. Dicken, W. Mérida, Measured effects of filling time and initial mass on the temperature distribution within a hydrogen cylinder during refuelling, J. Power Sources 165 (2007).

[23] B. Launder, D. Spalding, Lectures in Mathematical Models of Turbulence, Academic Press, London; New York, 1972.

[24] M. Monde, Y. Mitsutake, P.L. Woodfield, S. Maruyama, Characteristics of heat transfer and temperature rise of hydrogen during rapid hydrogen filling at high pressure, Heat Transf. Asian Res. 36 (1) (2006) 13–27.

[25] Toyota, 2017 Mirai product information, 2017, https://media.toyota.co.uk/wp-content/files_mf/1444919532151015MToyotaMiraiTechSpecFinal.pdf. (Accessed 20 April 2020).

[26] M. Striednig, S. Brandstätter, M. Sartory, M. Klell, Thermodynamic real gas analysis of a tank filling process, Int. J. Hydrogen Energy 39 (16) (2014) 8495–8509.

[27] B. Petukhov, Heat Transfer and Friction in Turbulent Pipe Flow with Variable Physical Properties, in: Advances in Heat Transfer, vol. 6, Elsevier, 1970, pp. 503–564.

[28] P.L. Woodfield, M. Monde, Y. Mitsutake, Measurement of averaged heat transfer coefficients in high-pressure vessel during charging with hydrogen, nitrogen or argon gas, J. Therm. Sci. Technol. 2 (2) (2007) 180–191.

[29] J.W. Leachman, R.T. Jacobsen, S.G. Penoncello, E.W. Lemmon, Fundamental equations of state for parahydrogen, normal hydrogen, and orthohydrogen, J. Phys. Chem. Ref. Data 38 (3) (2009) 721–748.

[30] C.D. Muzny, M.L. Huber, A.F. Kazakov, Correlation for the viscosity of normal hydrogen obtained from symbolic regression, J. Chem. Eng. Data 58 (4) (2013) 969–979.

[31] M.J. Assael, J.-A.M. Assael, M.L. Huber, R.A. Perkins, Y. Takata, Correlation of the thermal conductivity of normal and parahydrogen from the triple point to 1000 K and up to 100 MPa, J. Phys. Chem. Ref. Data 40 (3) (2011) 033101.